PHYSICAL REVIEW B VOLUME 5, NUMBER 8 15 APRIL 1972

Weak Absorption Tails in Amorphous Semiconductors

D. L. Wood
Bell Laboratories, Murray Hill, New Jersey 07974

and

J. Tauc
Division of Engineering, Brown University, Providence, Rhode Island 02912
and Bell Laboratories, Murray Hill, New Jersey 07974

(Received 14 October 1971)

Optical absorption measurements near the absorption edge are presented for three bulk semiconductor glasses: As_2S_3, $Ge_{33}As_{12}Se_{55}$, and $Ge_{28}Sb_{12}Se_{60}$. The weak absorption tails observed below the exponential part of the edge also follow an exponential law, and they are not due to a light-scattering artifact. We associate them with localized states in the band gap. The results are interpreted in terms of a model in which optical transitions occur between localized states below the mobility edge and extended states of the opposite band.

INTRODUCTION

Amorphous semiconductors exhibit absorption edges which are usually situated in approximately the same energy range as the absorption edge of the crystalline form having a similar short-range order. Below this edge, the transparency of amorphous semiconductors can be remarkably high, at least until the frequencies of lattice vibrations become important. We present new experimental data on the absorption close to the edge and discuss the results in terms of localized states in the gap.

Absorption edges of amorphous semiconductors are often much more sensitive to the conditions of preparation, thermal history, and purity than the broad features of the whole optical absorption band. This holds in particular for thin films. A typical example is the absorption edge in amorphous Ge, which was found at different energies and with different shapes in films prepared by vacuum deposition, by sputtering, or by electrolytic methods. The edge of vacuum-deposited films can be shifted and sharpened by annealing,[1] but crystalline thin films sometimes show a similar behavior because of a large concentration of defects introduced into them during the deposition.[2] It appears that, if films of amorphous Ge are prepared or annealed after preparation so that they contain a small concentration of defects, the edge is quite sharp and the material is very transparent below the edge.[3] It is, however, difficult to measure the optical constants in this region with sufficient precision because the films are too thin.

The difficulties are less serious in materials which can be prepared in the amorphous state in the bulk form. In such materials it appears that the absorption edge can be reproduced more easily than in thin films, if the purity of the materials is kept high. We chose for our work vitreous As_2S_3, $Ge_{33}As_{12}Se_{55}$, and $Ge_{28}Sb_{12}Se_{60}$, which are also available commercially as homogeneous optical glasses.

In chalcogenide and some compound glasses in the strong absorption region of the edge (part A in Fig. 1, $\alpha > 10^4$ cm^{-1}), the absorption constant α can be described by the relation

$$\hbar\omega\alpha \sim (\hbar\omega - E_g^{\mathrm{opt}})^r , \tag{1}$$

where the constant r is usually equal to 2 or 3, and E_g^{opt} is the optical band-gap energy.[4,5]

Below $\alpha \approx 10^4$ cm^{-1} the absorption constant is larger than the value obtained from Eq. (1), and the edge is broadened. For α between 1 and 10^4 cm^{-1} (part B in Fig. 1) it has been observed in all compound semiconducting glasses so far studied that

$$\alpha \sim e^{\hbar\omega/E_1} , \tag{2}$$

where E_1 is in the range 0.05–0.08 eV in various glasses below and at room temperature, while above room temperature E_1 increases with temperature.

At very low absorption levels ($\alpha < 1$ cm^{-1}) one observes another exponential part of the absorption edge (weak absorption tail, part C in Fig. 1) where

$$\alpha \sim e^{\hbar\omega/E_t} \tag{3}$$

and the energy E_t is always larger than E_1.

In contrast to part B which is similar in different materials and easily reproducible, part C is a structure-sensitive property. Vaško[6] studied this part in amorphous Se and showed that it depended on the purity and perfection of the material. The weak absorption tail has also been observed in As_2Se_3, As_2SeTe_2, and As_2Se_2Te glasses[7] and in As_2S_3 glass.[8] The sensitivity of the weak absorption tail to the purity and method of preparation appears

TABLE I. Analytical results for chalcogenide glasses; semiquantitative analyses, in ppm.

	Fe	Pb	Cu	Al	Si	Mg	Sb	Ca	V
Servofrax As_2S_3	10-50	1-5	1-10	1-5	1-5	1-5	100-1000	•••	•••
BTL As_2S_3 #8	1-10	1-10	1-5	1-5	1-5	1-10	•••	•••	•••
#20	1-5	1-5	1-5	•••	•••	1-5	•••	•••	•••
#21	1-5	1-10	1-10	1-10	1-5	1-10	•••	•••	•••
Orpiment As_2S_3	1-10	1-10	•••	1-10	1-10	1-10	•••	•••	•••
TI 20[a]	1-5	•••	•••	1-5	1-5	1-5	•••	1-5	•••
TI 1173[b]	1-10	•••	1-5	1-5	1-10	1-5	major	1-5	1-5

[a]TI 29 nominal: $Ge_{33}As_{12}Se_{55}$; found: $Ge_{33}As_{11.1}Se_{56.0}$. [b]TI 1173 nominal: $Ge_{28}Sb_{12}Se_{60}$; found: $Ge_{28}Sb_{12.9}Se_{61.9}$.

to indicate that this part of the absorption edge in chalcogenide glasses corresponds to defect-induced absorption.

We present data on the weak absorption tail for three chalcogenide glasses and show that it is not an artifact due to light scattering. We discuss the results in terms of absorption associated with localized energy states in the band gap.

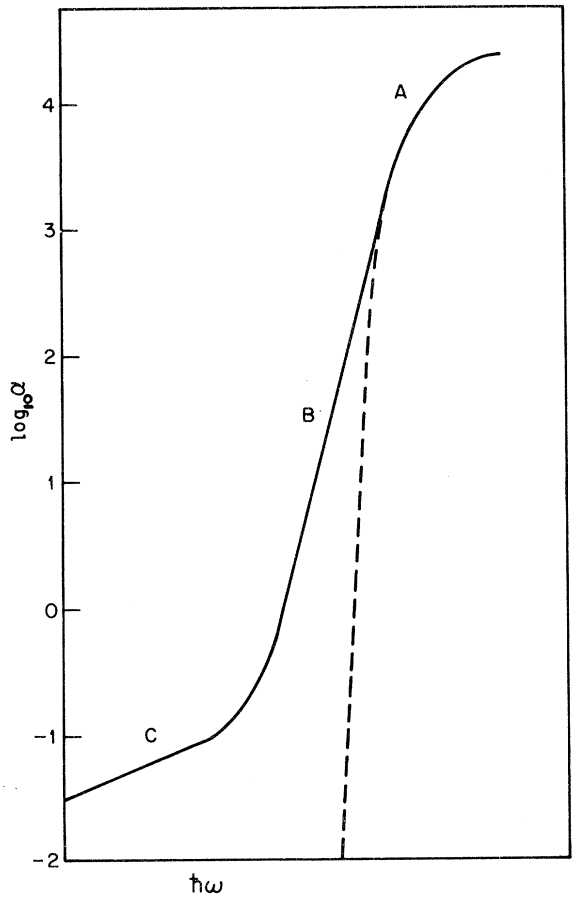

FIG. 1. A, B, and C. The three principal regions of optical absorption in an amorphous semiconductor. Dashed line represents extrapolation of part A, using Eq. (1) (see text).

EXPERIMENTAL

The three materials on which we report results are available from commercial sources. We used As_2S_3 from Servo Corporation, available under the name Servofrax. The other two came from TI with the designation of Glass #20 ($Ge_{33}As_{12}Se_{55}$) or Glass #1173 ($Ge_{28}Sb_{12}Se_{60}$). We also used some very pure As_2S_3 samples prepared in a rocking furnace at Bell Laboratories by Menth for magnetic susceptibility measurements.[9,10] The samples were prepared for optical measurement in the form of cylinders about 16 mm in diameter and of varying lengths from 20 mm to less than 0.02 mm. The end surfaces of the cylinders were ground and polished by standard optical finishing techniques, ending with a final polish with very fine alumina powder (Linde B). The ends of the cylinders were maintained parallel to about 2 min, since a wedge larger than that produced differences in absorption as large as those being measured in the particular spectrophotometer being used. With the commercial samples there was no trouble with refractive index inhomogeneities, but we had to be careful with our own samples to avoid difficulties from this deficiency. For the Texas Instruments Company (TI) glasses it was not necessary to be so careful because the weak absorption tails in which we were interested occurred at much higher absorption levels ($\alpha > 0.12$ cm^{-1}) than for the As_2S_3 ($\alpha > 0.02$ cm^{-1}).

For measurement of the very low absorption values observed for As_2S_3, we found it convenient to plot thickness against optical density for a series of samples of increasing thicknesses in order to achieve more reliable results. The slope of the curve obtained gave the absorption coefficient directly for each wavelength. Even at the higher absorption values, we used more than one thickness for each wavelength in order to enhance the consistency of the results.

Because it was desirable to correlate the magnetic susceptibility and optical data, it was of great importance to monitor the purity of the samples used. The analytical results for the samples we studied are given in Table I. We conclude that

none of the glass samples contained more than about 50 ppm of total impurities, except for the commercial As_2S_3 which contained about 500 ppm of Sb and appreciably more Fe than the rest. The quantitative results for the major constituents of the TI glasses are expressed as the atomic formula, having been translated from the raw weight percent data. These are particularly difficult analyses, and the accuracies of the nominal formulas representing the starting recipe are probably better than those of the analyses.

LIGHT-SCATTERING MEASUREMENTS

At the very low absorption levels observed, it is necessary to be assured that no other optical losses besides true absorption are occurring. In particular, the loss due to light scattering from particles can be very troublesome. To evaluate this factor we made direct measurements of the light-scattering loss for representative samples of each material by means of a modification of the integrating cube scattering detector.[11] In our version of the method the glass is cut into a 1-cm cube with six optically finished surfaces and placed in a cavity lined with five solar-cell photodetectors having 1-cm-square surfaces, as shown in Fig. 2. Radiation from a monochromator falls on the open sixth face of the cavity through a circular or square aperture, and the intensity of radiation falling on the solar cell opposite the entrance aperture measures the transmitted component. The total intensity falling on the four solar cells around the periphery measures the scattered component and the fifth solar cell was removed for the latter measurement, as scattering of the exit beam may otherwise reach the peripheral detectors. The actual experiment, therefore, is extremely simple, but there are several important corrections that must be made in order to convert the measured ratio of transmitted to scattered radiation into the true scattering coefficient for the material, β. β is defined through the relationship

$$dI_s = \frac{\beta I\, dV}{A} = \beta I\, dx\,, \tag{4}$$

where dI_s is the radiation scattered from a volume element $dV = A\, dx$ and I/A is the radiation flux density incident on the volume element. With this definition β is directly comparable with the absorption constant α, in Lambert's law, and

$$I = I_0 e^{-(\alpha+\beta)x} \tag{5}$$

describes the attenuation of radiation in passing through the material.

The first correction to the scattering ratio involves the reflection of radiation at the glass-air interface, where this acts to reduce both the transmitted and the scattered components at the exit surfaces of the cube. The corrections for these two losses cancel for the measured ratio of scattered to transmitted intensity. However, the reflection of the tranmitted beam at the rear surface of the glass cube also produces scattering, and a fraction $\rho = (n-1)^2/(n+1)^2$ must be added to the intensity of the incident radiation. A second component reflected at the front face also contributes to the scattering but the appropriate factor (ρ^2) is small compared with ρ even for the large indices of refraction of the chalcogenide glasses ($2 < n < 3$).

In addition to the reflection, there are two corrections due to optical absorption at the wavelengths of interest. One involves the attenuation of the incident radiation in passing through the cube, and the other involves the attenuation of the scattered radiation as it passes out of the cube. These two factors contribute appreciably only where the absorption coefficient is large ($\alpha > 1$), and for larger values where $\beta \ll \alpha$ we obtained a factor $\alpha^2/(1-e^{-\alpha})^2$ for a cube of 1-cm dimensions and where α is the absorption constant at the particular wavelength.

For most of the wavelength region of interest, the largest correction factor comes from the fact that at appreciable angles of incidence ($i > 22°$) the scattered radiation is totally internally reflected by the exit face of the cube. Thus, for an elemental unit volume within the glass only the scattered radiation within a cone of half-angle equal to the critical angle of reflection escapes from each cube and is collected by a detector. This can be reduced for our simplified geometry to a factor (n^2-1), where n is the refractive index.

On combining all these correction factors and letting I_s/I_t be the measured ratio of scattered intensity relative to the transmitted intensity, we obtained for the scattering coefficient for a rectangular parallelopiped with dimensions $h \times h \times l$ and the radiation propagated along the dimension l,

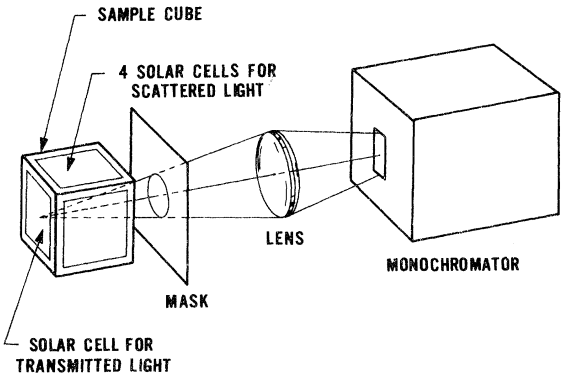

FIG. 2. Experimental arrangement for measuring light scattering in bulk samples of amorphous semiconductors.

TABLE II. Light-scattering data for chalcogenide glasses.

	λ, μm	ħω, eV	I_0/I_s	Correction Factor	β, cm^{-1}
Servo-frax	0.6	2.06	770	78.48	0.102
	0.6328	1.96	750	13.37	0.0178
	0.65	1.91	730	10.58	0.0144
	0.7	1.77	685	8.55	0.0125
	0.75	1.76	645	7.86	0.0122
	0.8	1.55	600	7.43	0.0124
	0.85	1.46	560	7.21	0.0128
	0.9	1.38	515	7.01	0.0136
	0.95	1.31	468	6.9	0.0147
	1.0	1.24	430	6.8	0.0158
	1.05	1.18	385	6.6	0.0171
	1.1	1.13	340	6.5	0.0191
TI 20	0.75	1.65	286	182	0.636
	0.8	1.55	245	25	0.102
	0.85	1.46	219	14.4	0.066
	0.9	1,38	213	11.96	0.056
	0.95	1.31	216	10.82	0.050
	1.0	1.24	222	10.16	0.046
	1.05	1.18	227	9.64	0.042
	1.1	1.13	204	9.32	0.046
TI 1173	8.9	1.38	288	71.9	0.249
	0.95	1.31	258	18.2	0.070
	1.0	1.24	232	14.0	0.060
	1.05	1.18	222	12.6	0.057
	1.1	1.13	202	11.9	0.059

$$\beta=\left(\frac{I_s}{I_t}\right)\frac{6}{4}\,\frac{1}{(1+\rho)}\,(n^2-1)\,\frac{\alpha}{(1-e^{-\alpha l})}\,\frac{\alpha h}{(1-e^{-\alpha h})}\,, \quad (6)$$

where the factor $\frac{6}{4}$ appears because only four of the six cube faces are fitted with scattering detectors, ρ is the reflection coefficient for a glass-air surface, n is the refractive index, and α is the absorption constant.

Our results for the three materials studied are given in Table II, where it can be seen that even though the correction factor is rather large for large values of α, the scattering coefficient β is small compared with the absorption coefficient, and the weak absorption we measured is not an artifact.

OPTICAL ABSORPTION RESULTS

The results obtained on three chalcogenide glasses for room-temperature samples are shown in Fig. 3 and the values are given in Table III. The two linear segments of each curve corresponding to parts B and C of the generalized curve of Fig. 1 can be represented quite well by a relation of the form $\alpha=A_t\,e^{\hbar\omega/E_t}+A_1e^{\hbar\omega/E_1}$ with the coefficients given in Table IV. The fit is not perfect in the knee of the curve, but of course is best for the linear segments. The coefficients E_1 which express the slope of the upper portion of the curves have values in the range $0.05<E_1<0.08$ already mentioned as applying to a wide range of compounds. The slopes determined by E_t are more variable, and this segment of the curves, at low α values, is the one which varied from one compound to another, and which reveals information about the structure of each material. We have found that the values of α for As_2S_3 in the weak absorption tail are somewhat lower for very pure As_2S_3 (BTL #31) than for Servofrax containing about 0.05% Sb.

DISCUSSION

We shall discuss our data using the model of the band-state densities in amorphous semiconductors suggested by Mott and others[12,13] (Fig. 4). Our

TABLE III. Optical absorption of chalcogenide glasses.

λ, μm	E, eV	Servofrax As_2S_3 α, cm^{-1}	BTL 31 As_2S_3 α, cm^{-1}	λ, μm	E, eV	TI 20 $Ge_{33}As_{12}Se_{55}$ α, cm^{-1}	TI 1173 $Ge_{28}Sb_{12}Se_{60}$ α, cm^{-1}
0.56	2.22	53		2.5	0.50	0.15	0.30
0.57	2.18	21		2.0	0.62	0.16	0.32
0.58	2.14	12.2		1.5	0.82	0.19	0.37
0.59	2.10	6.0	6.14	1.3	0.95	0.24	0.39
0.60	2.06	3.1	3.06	1.1	1.12	0.26	0.44
0.61	2.04	1.74	1.73	1.0	1.24	0.40	0.60
0.62	2.00	1.04	1.01	0.95	1.30	0.47	0.90
0.63	1.97	0.70	0.62	0.90	1.38	0.53	1.87
0.64	1.94	0.52	0.44	0.85	0.46	1.73	7.22
0.65	1.91	0.41	0.32	0.80	1.55	1.38	38
0.66	1.88	0.33	0.25	0.75	1.65	4.2	144
0.67	1.85	0.28	0.21	0.70	1.77	29	748
0.70	1.77	0.21	0.138	0.68	1.82	51	
0.72	1.72	0.18	0.115	0.66	1.88	110	
0.74	1.68	0.134	0.092	0.64	1.94	285	
p.76	1.63	0.122	0.092	0.62	2.00	614	
0.78	1.59	0.104	0.07	0.60	2.06	1462	
0.80	1.55	0.097	0.06				
1.0	1.24	~0.03	~0.02				

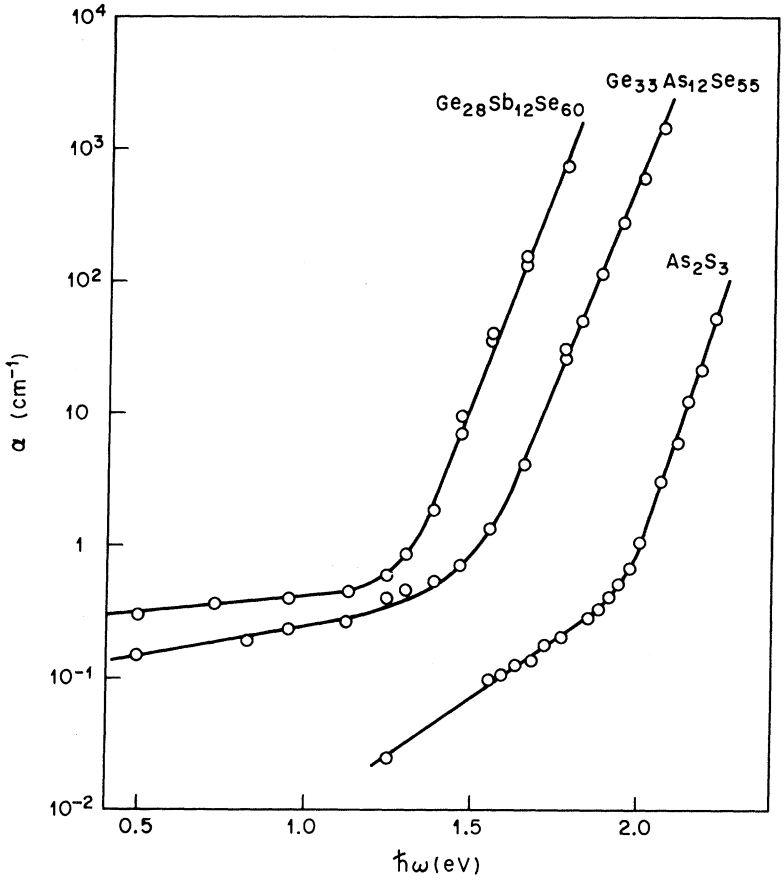

FIG. 3. Optical absorption vs photon energy for three amorphous semiconductor glasses at room temperature. The As_2S_3 samples were Servofrax. The $Ge_{28}Sb_{12}Se_{60}$ is Glass # 1173 and the $Ge_{33}As_{12}Se_{55}$ is Glass # 20 both of Texas Instruments Company.

distinction between the band states and the tail states is based on the form of the energy dependence of their densities. The band states correspond to the bonding states in the valence band and the antibonding states in the conduction band in an "ideal" glass. We shall call a glass ideal if it has all chemical bonds satisfied. The tail states may correspond to the defects in this ideal structure such as dangling bonds, but, alternatively, similar states may be present even in an ideal glass. In this case, they correspond to deep potential fluctuations in the disordered structure. The exact nature of the tail states has not been classified yet. Empirically, we may distinguish between the states due to the ideal structure and those due to defects by the greater sensitivity of the latter to annealing. There is no deeper justification for this, and indeed, there may be little difference, if any, between the deep states in an ideal structure and a defect state. The band states are localized below the mobility edge and extended at energies above the mobility edge.

TABLE IV. Coefficients for $\alpha = A_t\, e^{\hbar\omega/E_t} + A_1\, e^{\hbar\omega/E_1}$ in chalcogenide glasses.

Material	A_t(cm^{-1})	A_1(cm^{-1})	E_t(eV)	E_1(eV)
Servofrax As_2S_3	5.65×10^{-4}	2.02×10^{-15}	0.30	0.059
TI 20	0.077	3.77×10^{-10}	0.84	0.071
TI 1173	0.211	2.28×10^{-8}	1.56	0.066

Part A of the absorption edge (Fig. 1) is undoubtedly due to transitions between the band states. The exponential shape of parts B and C suggest that they are associated with the tail states. Transitions between localized states are considerably less probable than transitions between extended states or between a localized state and extended states. We shall assume that the absorption is due to the latter process, using formula (7) for the absorption constant.[14] This assumption is in agreement with the observation by Kolomiets *et al.*[15] of photoconductivity in the wavelength range concerned. Thus,

$$\alpha(\omega) = \frac{\pi^2 e^2 \hbar}{mc}\,\frac{f}{n} \times \int_{(\hbar\omega_{\max}-\hbar\omega)}^{\infty} V(E_i)N(E_i)g(\hbar\omega - \hbar\omega_{\max} + E_i)\,dE_i \ . \tag{7}$$

This equation was deduced under the assumption that the optical transitions take place from localiz-

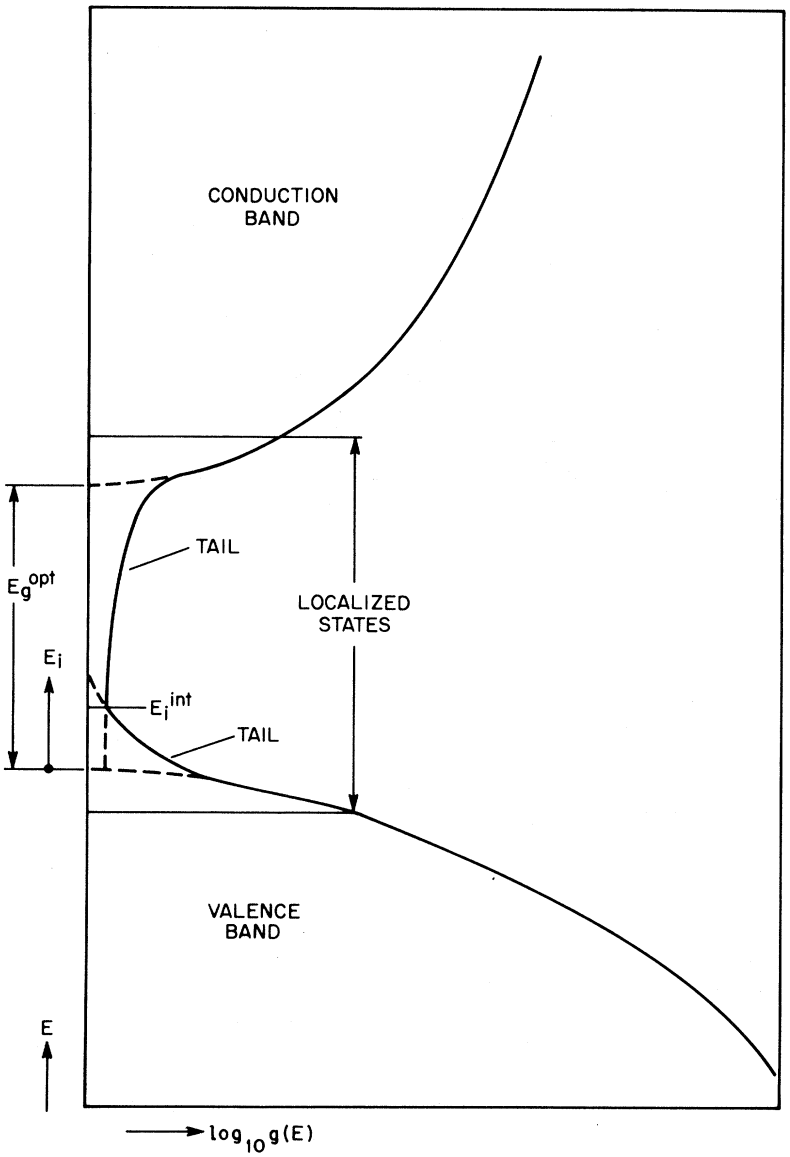

FIG. 4. Schematic diagram of the density of states for an amorphous semiconductor. The range for $g(E)$ covers many orders of magnitude.

ed states with the state density $N(E_i)$ (Fig. 4) to the extended states of the opposite band with the state density $g(E)$ or vice versa; during the transitions only energy is conserved. The volume over which the state is localized is $V(E_i)$. $\hbar\omega_{max}$ is the maximum energy in the optical absorption associated with the tail, and it appears reasonable to assume it equal to E_g^{opt} defined in Eq. (1). n is the index of refraction and f is the oscillator strength. Both are considered constant over the energy range considered.

We have assumed that the wave functions of the localized states can be described as linear combinations of the wave functions in the adjacent band in the corresponding crystal. Under this assumption, f is the same as for transitions from the top of one band to the bottom of the next in the corresponding crystal. Its order of magnitude is 1 in the crystal. Equation (7) can be well justified in a crystal for transitions from a localized state with energy level close to one band edge into the opposite band. A similar formula gave a very good agreement with experiment for optical transitions in crystalline GaAs.[16]

Davis and Mott[5] argue that in amorphous semiconductors $V(E_i)$ should be independent of E_i and approximately equal, in our notation, to the volume of the elementary unit cell V_0. This follows also from the random-phase model as discussed by Hindley.[17] The experimental evidence seems to be in accord with very small values of V.[14] The applicability of Davis and Mott's argument is not

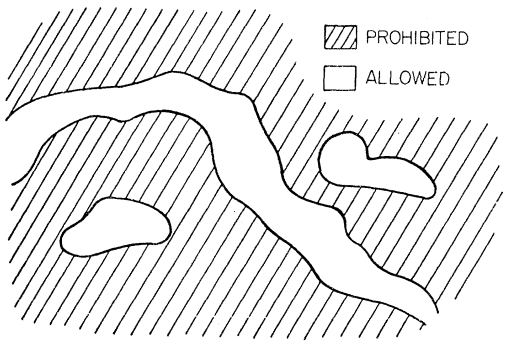

FIG. 5. Regions of allowed and prohibited states in an amorphous semiconductors just above the mobility edge.

proven in our case, but we consider it plausible and take $V(E_i) = V_0$ independent of E_i.

We now assume that

$$N(E_i) = NE_t^{-1}\,[1 - \exp(-E_{i\ \max}/E_t)]^{-1} e^{-E_i/E_t}, \quad (8)$$

where N is the total concentration of states between $E_i = 0$ and $E_i = E_{i\max}$. It follows from Eq. (7) that

$$\alpha(\omega) = \alpha_{\max} \exp[-(\hbar\omega_{\max} - \hbar\omega)/E_t], \quad (9)$$

$$\alpha_{\max} = \frac{\pi^{5/2} e^2 \hbar}{2mc} \frac{f}{n} g(E_t) V_0 N [1 - \exp(-E_{i\max}/E_t)]. \quad (10)$$

Formula (9) describes within the precision of measurement $\alpha(\omega)$ in the regions B and C with the parameters given in Table V. The density of states $g(E)$ was taken equal to the free electron density:

$$g(E) = 4\pi(2m/h^2)^{3/2} E^{1/2}. \quad (11)$$

V_0 is of the order of the molecular volume (10^2 Å^3). Assuming $f \approx 1$, we obtain the order of magnitude of the total concentration of the states associated with part B, $N_B \approx 10^{20}$ cm^{-3}, and for the states associated with part C, $N_C \approx 10^{16} - 10^{17}$ cm^{-3}.

It is impossible to assign part B or part C to definite transitions on the basis of optical data alone. If we arbitrarily associate part B with transitions involving the valence band tail and part C with transitions involving the conduction band tail, we obtain the density of states at the intersection of both tails $N(E_i^{\rm int})$ and the Fermi level E_i^F, as quoted in Table V. They were calculated with the assumption that $f V_0 = 10^2$ Å^3.

It appears, however, that this simple interpretation of part B is incorrect and that part B may be better described as a broadening of the part of the curve following Eq. (1) (part A in Fig. 1). The exponential edges observed in some crystals as Urbach tails are basically similar to part B in amorphous semiconductors. It seems therefore plausible to associate the exponential edges with similar mechanisms in both cases.[18,19] With this interpretation, the densities $N(E_i)$ for part B deduced from the optical data as above are not actual densities of states because it is not possible to assume $f \approx 1$. The transition probabilities will be reduced[20] by a factor depending on the overlapping of the wave functions in the initial and final states, and will be energy dependent.

The absorption in part C corresponds to transitions from localized states deep in the gap to the extended states. In this interpretation part C is associated with deep potential fluctuations and part B is associated with relatively extended but shallow potential fluctuations (of the order of 0.1 eV, cf. the recent work by Nielsen[21] on photoemission from amorphous As_2Se_3). The deep potential fluctuations may be due to disorder, defects, or impurities.

The concentration of states corresponding to part C was estimated above to be 10^{16}–10^{17}/cm^3. This is a very low concentration, one or two orders of magnitude smaller than the total concentration of impurities given in Table I or estimated from the measurement of magnetic susceptibilities.[10] A similar discrepancy has been noticed when the optically determined state densities were compared with the densities from transport effects.[22] The reason for this discrepancy may be that the energies of the impurity states are close to the band edges and do not significantly contribute to part C. In any case the concentration of states in the gap induced by disorder appears to be quite low. However, it can be one or two orders of magnitude higher than the estimate because of the Dow-Hopfield[20] electron-hole correlation effect which reduces the effective optical absorp-

TABLE V. Parameters in Eqs. (9) and (10).

Material	$E_g^{\rm opt}$ eV	n	Part B E_t eV	Part B $\alpha_{\max}$ cm^{-1}	Part B fV_0N^a	Part C E_t eV	Part C $\alpha_{\max}$ cm^{-1}	Part C fV_0N^a	Part C fV_0N^b	E_i^F eV	$E_i^{\rm int}$ eV	$N(E_i^{\rm int})$ cm^{-3}eV^{-1}
As_2S_3	2.36	2.60	0.059	400	1.3×10^{-2}	0.30	1.0	14×10^{-6}	14×10^{-6}	0.72	0.80	2.6×10^{15}
$Ge_{33}As_{12}Se_{55}$	1.96	2.49	0.071	400	1.1	0.84	0.8	6.5	4.5	0.64	0.80	2.0×10^{16}
$Ge_{28}Sb_{12}Se_{60}$	1.72	2.60	0.066	400	1.2	1.56	0.6	3.8	1.5	0.58	0.78	1.3×10^{16}

[a]Calculated for $E_{i\max} = \infty$.

[b]Calculated for $E_{i\max} = E_g^{\rm opt}/2$.

tion cross section. In this interpretation the internal electric fields[19,22] make the glasses more transparent than a crystal with the same concentration of states in the gap. One can roughly visualize the nature of the effect with the following picture. As the percolation theory suggests,[23] above the mobility edge, but close to it, the extended states do not exist in the whole volume V_s of the sample but only in a part V_s' (Fig. 5). If we neglect transitions between states located at different sites, the absorption is reduced by a factor V_s'/V_s.

ACKNOWLEDGMENTS

We are grateful to Miss B. E. Prescott and J. Waszczak for technical assistance, and to Professor J. D. Dow and Dr. A. Menth for many helpful discussions. We thank Professor H. Fritzsche and Dr. P. Nielsen for the preprints of their papers.

[1]M. L. Theye, Mater. Res. Bull. 6, 103 (1971).
[2]J. E. Davey and T. Pankey, J. Appl. Phys. 40, 212 (1969).
[3]T. M. Donovan, W. E. Spicer, J. M. Bennett, and E. J. Ashley, Phys. Rev. B 2, 397 (1970).
[4]J. Tauc, in *The Optical Properties of Solids*, edited by F. Abeles (North-Holland, Amsterdam, 1971).
[5]E. A. Davis and N. F. Mott, Phil. Mag. 22, 903 (1970).
[6]A. Vaško, in *Physics of Selenium and Tellurium*, edited by W. C. Cooper (Pergamon, New York, 1969), p. 241.
[7]J. T. Edmond, Brit. J. Appl. Phys. 17, 979 (1966).
[8]E. L. Zorina, Opt. i Spektroskopiya 27, 320 (1969) [Opt. Spectry. (USSR) 27, 168 (1969)]; P. A. Young, J. Phys. C 4, 93 (1971). These two authors ascribe the weak absorption tails (which they observed at absorption levels very different from each other) to indirect phonon-assisted transitions. However, the observed temperature dependence cannot be explained by the current theory of such transitions.
[9]J. Tauc and A. Menth, Bull. Phys. Soc. 15, 553 (1970).
[10]A. Menth, F. DiSalvo, and J. Tauc (unpublished).
[11]A. R. Tynes, Appl. Opt. 9, 2706 (1970).
[12]N. F. Mott, Phil. Mag. 13, 989 (1966).
[13]M. H. Cohen, H. Fritzsche, and S. R. Ovshinsky, Phys. Rev. Letters 22, 1065 (1969).
[14]J. Tauc, A. Menth, and D. L. Wood, Phys. Rev. Letters 25, 749 (1970).
[15]B. T. Kolomiets, T. F. Mazets, and Sh. M. Efendiev, J. Non-Cryst. Solids 4, 95 (1970).
[16]D. M. Eagles, J. Phys. Chem. Solids 16, 76 (1960).
[17]N. K. Hindley, J. Non-Cryst. Solids 5, 17 (1970).
[18]J. Tauc, Mater. Res. Bull. 5, 721 (1970).
[19]J. D. Dow and D. Redfield, Phys. Rev. Letters 26, 762 (1971).
[20]J. D. Dow and J. J. Hopfield, Proceedings of the Fourth International Conference on Amorphous and Liquid Semiconductors, Ann Arbor, Mich., 1971 (unpublished).
[21]P. Nielsen, Solid State Commun. 9, 1745 (1971).
[22]H. Fritzsche, J. Non-Cryst. Solids 6, 49 (1971).
[23]M. H. Cohen, J. Non-Cryst. Solids 4, 391 (1970).

PHYSICAL REVIEW B VOLUME 5, NUMBER 8 15 APRIL 1972

Phonon Density of States in Germanium at 80 K Measured by Neutron Spectrometry

G. Nelin and G. Nilsson
Aktiebolaget Atomenergi, Studsvik, Sweden
(Received 29 July 1971)

More than 500 frequencies of phonons with reduced wave vectors evenly distributed over an irreducible section of the first Brillouin zone have been measured in germanium at 80 K with a neutron crystal spectrometer. The phonon density of states was calculated from the data with an improved sampling technique. Comparisons between thermodynamic quantities derived from calorimetric data and from the present spectrum reveal an excellent agreement. A critical-point scheme determined by use of a method originating from Phillips is also presented. The scheme properly satisfies the Morse relations and other topological conditions, and most of the van Hove singularities expected are clearly displayed in the spectrum.

I. INTRODUCTION

The phonon density of states $g(\nu)$ of a crystalline solid is defined as follows. The function $g(\nu)d\nu$ signifies the fraction of the total number of phonon states in the frequency interval $(\nu, \nu+d\nu)$ if $\int g(\nu)d\nu$ is normalized to 1. Knowledge of $g(\nu)$ is essential for understanding of the thermodynamic properties, for extraction of the electron-phonon coupling coefficient in a tunnel-junction experiment, for design of reactor moderators, etc. It is difficult to make good direct measurements of the density of states, and few spectra have actually been studied. Usually measurements reveal only the main peaks.